Thickness Dependent Phase Behavior of Antiferroelectric Liquid Crystal Films

LiDong Pan,[1] Shun Wang,[1] C. S. Hsu,[2] and C. C. Huang[1]

[1]*School of Physics and Astronomy, University of Minnesota, Minneapolis, Minnesota 55455, USA*
[2]*Department of Applied Chemistry, National Chiao Tung University, Hsinchu 30050, Taiwan*

(Received 8 June 2009; published 30 October 2009)

Free standing films of a liquid crystal compound with simple surface enhanced order were studied. The resultant phase diagram demonstrates that (1) the short helical pitch smectic-C^*_α phase disappears below a film thickness of 10 layers, and (2) the temperature window of a distorted 4 layer smectic-C^*_{FI2} phase increases dramatically upon decreasing film thickness. The experimental findings were attributed to the reduced dimensionality and enhanced surface effects in thin films. The results of the smectic-C^*_α phase are consistent with what have been reported for helically ordered magnetic thin films, with a noticeable difference due to the opposite effect of the surface on ordering in the two systems.

DOI: 10.1103/PhysRevLett.103.187802 PACS numbers: 61.30.Hn, 64.70.M−, 77.84.Nh

With the discovery of chiral antiferroelectric liquid crystal (AFLC) materials, several new smectic phases below smectic-A (SmA, in which long axes of the molecules are parallel to the layer normal) were identified [1]. Since in those new phases, molecules are all tilted, they are usually referred to as the smectic-C^* (SmC^*) variant phases. The successful application of a resonant x-ray diffraction technique [2] and optical probes [3] established the molecular arrangements called the ''distorted clock model.'' Different SmC^* variant phases are characterized with different azimuthal arrangements of tilt directions among layers. Within each layer, the tilt directions are uniform if no defects are present. For example, smectic-C^*_α (SmC^*_α) and SmC^* phases are featured with a helical structure with pitch on the order of nanometers and micrometers, respectively, while smectic-C^*_{FI2} (SmC^*_{FI2}) and smectic-C^*_{FI1} (SmC^*_{FI1}) phases have 4-layer and 3-layer unit cell with structures discussed in detail in Ref. [3].

In order to understand the physical origins and the interactions responsible for the SmC^* variant phases, several theoretical models have been proposed [4–9]. However, there is still no theory that provides a comprehensive picture of the origin of the SmC^* variant phases, or the nature of the interactions responsible for them.

In this Letter, we reported our study on the thickness dependence of SmC^* variant phases from free standing films of one chiral AFLC compound. To the best of our knowledge, this is the first systematic study of thickness dependence of the stability of SmC^* variant phases. Previous studies of this kind either did not involve SmC^* variant phases [10] or used nondeterministic method [11]. Thus, we believe the results will provide new insight into our understanding of the nature of SmC^* variant phases and the interactions responsible for them.

The AFLC compound chosen for this study is (R)-MHPBC. Its molecular structure is shown at the top of Fig. 1. Phase sequence in bulk is isotropic (109 °C) − SmA (76 °C) − SmC^*_α (71 °C) − SmC^*_{FI2} (66 °C) − SmC^*_{FI1} (63 °C) − SmC^*_A. This compound was chosen for its simple surface structure. Previous study reported that MHPBC free standing films above the SmA − SmC^*_α transition show a simple surface induced tilt transition and have the surface phase thickness (L_S) ≤ 2 layers [12]. As comparison, some other AFLCs have $L_S \approx 9$ layers [13] or multiple surface transitions [14]. Thus, using MHPBC allows us to minimize the complicated surface effects.

In our null transmission ellipsometer (NTE) [15], optical parameter Δ is acquired. Δ measures the phase difference between the p and s component of the incident light necessary to produce linearly polarized transmitted light. The liquid crystal free standing films are prepared over a cover glass slide with a 4-mm diameter hole. Applying a proper set of voltages to eight evenly spaced electrodes

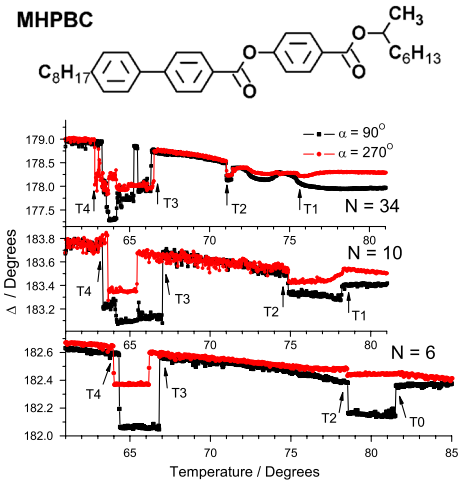

FIG. 1 (color online). Δ as a function of temperature upon cooling from films with thickness $N = 6$, 10, and 34 layers with $\alpha = 90°$ (black squares) and 270° (red dots). $T0$, $T1$, $T2$, $T3$, and $T4$ mark the transitions into SmC^*, SmC^*_α, SmC^*_{FI2}, SmC^*_{FI1}, and SmC^*_A phase. On the top is the chemical structure of MHPBC.

 © 2009 The American Physical Society

around the film hole creates a rotatable uniform in-plane dc electric field over the film. For films with nonzero in-plane polarization, the whole structure can be rotated smoothly about the layer normal by changing the direction of the electric field (**E**). Variable α denotes the angle between **E** and the projection of the laser's wave vector **k** onto the film plane.

Figure 1 shows the ellipsometric parameter Δ as a function of temperature upon cooling from the Sm*A* phase. The temperature ramp rate was 60 mK/ min. Data with **E** field orientation $\alpha = 90°$ (black squares) and $\alpha = 270°$ (red dots) are presented for films with thickness $N = 6$, 10, and 34 layers. In the figure, $T0$, $T1$, $T2$, $T3$, and $T4$ marks the transition into SmC^*, SmC^*_α, SmC^*_{FI2}, SmC^*_{FI1}, and SmC^*_A phase. These phases have the following characteristic features for parameter Δ. Above $T0/T1$, surface induced tilt produce a discernible difference between Δ_{90} and $\Delta_{270}(|\Delta_{270} - \Delta_{90}|_{\text{Surf}})$. Between $T1$ and $T2$, characteristic oscillation in Δ_{90} and Δ_{270} is the signature of SmC^*_α phase [16]. Because of the optically uniaxial structure of SmC^*_α phase, $|\Delta_{270} - \Delta_{90}|_{\text{Sm}C^*_\alpha} \leq |\Delta_{270} - \Delta_{90}|_{\text{Surf}}$. For the data between $T0$ and $T2$ of the 6-layer film, $|\Delta_{270} - \Delta_{90}|_{T0\text{ to }T2} > |\Delta_{270} - \Delta_{90}|_{\text{Surf}}$ indicates that it is the SmC^* phase. For data between $T2$ and $T3$; and data below $T4$, Δ_{90} matches Δ_{270} as temperature changes, this indicates a twofold rotational symmetry in the structure. Thus, the phases in these two regions are SmC^*_{FI2} and SmC^*_A. For data between $T3$ and $T4$, a noticeable difference between Δ_{90} and Δ_{270} was observed since the films were in a ferrielectric phase (SmC^*_{FI1}). Because the transitions at $T2$, $T3$, and $T4$ are all first order transitions, variations in transition temperatures are observed between different runs and are treated as uncertainties for the transition temperatures.

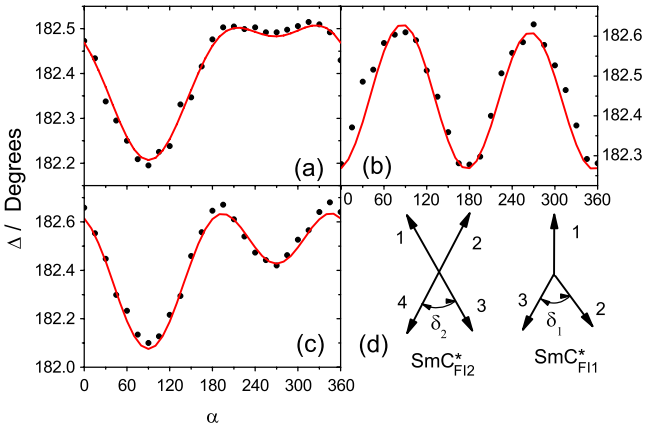

FIG. 2 (color online). Δ data (symbols) and fitting (lines) as a function of α from the 6-layer film at (a) $T = 80.3\,°\text{C}$ (Sm$C*$ phase), (b) $T = 67.6\,°\text{C}$ (SmC^*_{FI2} phase), (c) $T = 65.7\,°\text{C}$ (SmC^*_{FI1} phase). (d) Top views of structures for SmC^*_{FI2} and SmC^*_{FI1} phase, arrows represent the tilt direction of each layer, numbers represent the layer index within the unit cell.

In order to study the symmetries and structures of the phases in more detail and to confirm the results obtained from the temperature ramp, data were taken as a function of **E** field orientation α at various temperatures for several films. Shown in Figs. 2(a)–2(c) are Δ as a function of α from the 6-layer film at temperatures $T = 80.3\,°\text{C}$, $67.6\,°\text{C}$, and $65.7\,°\text{C}$. The solid lines are fitting results using a 4×4 matrix method [17]. Values of the principal indices of refraction and layer spacing used in the fitting are $n_o = 1.481 \pm 0.002$, $n_e = 1.626 \pm 0.01$, and $d = 3.44 \pm 0.05$ nm [12].

The structure used for the fitting in Fig. 2(a) is SmC^* with an anticlinic arrangement between two outermost layers. The tilt angle profile from surface to interior is: $11° \pm 2°$ (1st and 6th layer), $9° \pm 2°$ (2nd and 5th layer), and $8° \pm 2°$ (3rd and 4th layer). For Fig. 2(b), the structure used is SmC^*_{FI2} with an anticlinic surface [a top view of the SmC^*_{FI2} phase is shown in Fig. 2(d)]. For the fitting, $\delta_2 = 10° \pm 2°$ is used and an overall helix with pitch = 72 layers is added to the structure. The tilt angle profile used is: $18° \pm 2°$, $16° \pm 2°$, and $15° \pm 2°$ for Fig. 2(b) and $20° \pm 2°$, $17° \pm 2°$, and $16° \pm 2°$ for Fig. 2(c). The structure used for Fig. 2(c) is SmC^*_{FI1} with $\delta_1 = 60° \pm 10°$. Parameters δ_1 and δ_2 used for fitting the SmC^*_{FI1} and SmC^*_{FI2} structure are consistent with results from previous studies [3].

Free standing films of MHPBC with thicknesses ranging from 6 to 106 layers were studied. The resultant thickness dependent phase diagram obtained upon cooling from the Sm*A* phase is shown in Fig. 3. To avoid complications due to even-odd effect, for $N \leq 60$ layers, only films with even number of layers were chosen and studied. From the phase diagram, it is clear that all the transition temperatures show trends of increases upon decreasing N. $T1$ (transition into the SmC^*_α phase) shows a slight increase until $N < 10$ layers, where the SmC^*_α phase disappears and the SmC^*

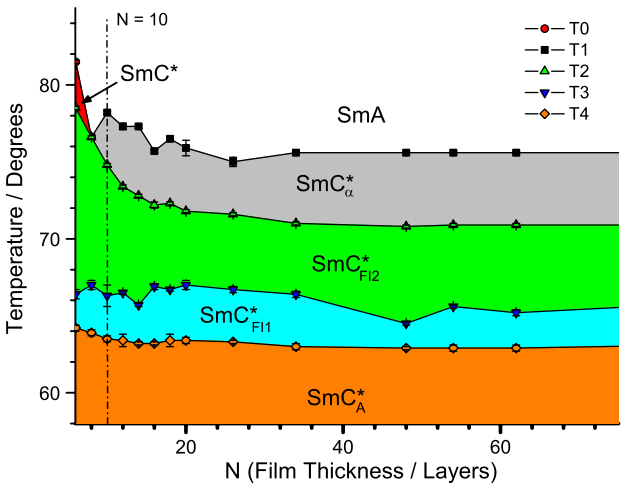

FIG. 3 (color online). Thickness dependent phase diagram of MHPBC free standing films obtained from cooling runs.

is observed instead. Upon decreasing N, $T2$ (transition into the SmC^*_{FI2} phase) increases dramatically, while $T3$ (transition into the SmC^*_{FI1} phase) and $T4$ (transition into the SmC^*_A phase) stay almost constant.

Figure 4(a) shows the temperature window of the SmC^*_α phase [ΔT(SmC^*_α)] as a function of N. ΔT(SmC^*_α) shows an overall trend of decrease upon decreasing N till below the 10 layer film, where the SmC^*_α phase completely disappears. The disappearing of the SmC^*_α phase in thin films has been observed in two other compounds [18,19]. However, in the 6-layer film of MHPBC, SmC^* structure is observed below SmA. A similar result was reported for the helical magnetic ordering temperatures (T_N) in Ho thin films [20]. E. Weschke *et al.* studied T_N as a function of film thickness by resonant magnetic soft x-ray and neutron diffraction. They found that T_N decreases with decreasing film thickness L and reaches 0 below a film thickness L_0 (10 monolayers) which is of the order of bulk helix period P_0 (7 to 12 monolayers as a function of temperature). The result was attributed to the reduced coordination number at the surface. A mean field model was employed to explain the results. From the calculation, it was also found that when T_N reaches 0 for $L \leq L_0$, the film is still magnetically ordered. A ferromagnetic structure exists below T_C, which is distinguishable from T_N only below L_0. Later, another group performed Monte Carlo simulations on the same system. The results agree with the mean-field calculation [21]. So far, the ferromagnetic structure in the films with T_N equals 0 has not been observed experimentally. Because of the structural similarities between helically ordered magnetic films and liquid crystal films in the SmC^*_α phase, our results can be viewed as an experimental confirmation of the prediction made for magnetic systems. Although due to the finite size effect, the ordering temperature for magnetic thin films is predicted to decrease as film thickness decreases; this is not observed for AFLC films. The most important reason for this is that for AFLC films, surfaces are usually more ordered than the interior and stronger surface interactions prevent the ordering temperature from decreasing.

The helical pitch of the SmC^*_α structure of MHPBC was previously determined to be about 7 layers [22]. Taking into account the surface layers, the film thickness at which the SmC^*_α phase disappears is of the order of the bulk helical pitch. In thinner films, the SmC^* structure is observed below SmA instead of SmC^*_α. Free energy of an N layer film having a helical structure can be written as

$$F = (N-1)J_1 \cos\phi + (N-2)J_2 \cos 2\phi \qquad (1)$$

with J_1 and J_2 being the coupling constants between the nearest-neighboring layers (NN) and next-nearest-neighboring layers (NNN), and ϕ being 2π divided by the helical pitch P_0. For the case of MHPBC, $J_1 = -2.5J_2$ gives a pitch value of 7 layers. Figure 4(b) shows the free energy per layer calculated from Eq. (1) with $J_1 = -2.5J_2$ for $\phi = 51.4°$ (SmC^*_α, black squares) and $\phi = 0$ (SmC^*, red dots). As shown in the figure, above a thickness of 6 layers, the SmC^*_α structure has lower energy, while below 6 layers, the SmC^* structure has lower energy, which is consistent with the experimental results. An intuitive explanation would be that in thin films, the weight of J_1 is more pronounced than J_2 since there are fewer NNN bonds than NN bonds, so that a longer helix is favored.

Figure 5(a) shows the temperature window of the SmC^*_{FI2} phase [ΔT(SmC^*_{FI2})] as a function of N. ΔT(SmC^*_{FI2}) increases dramatically as N decreases, especially for $N < 20$ layers.

In order to understand the enhanced stability of SmC^*_{FI2} phase in thin films, we studied the behavior of free energy per layer as a function of N. $|F|/N$ is an estimate of the average energy required to flip the orientation of a random layer in the structure; thus, it is a rough calculation of the

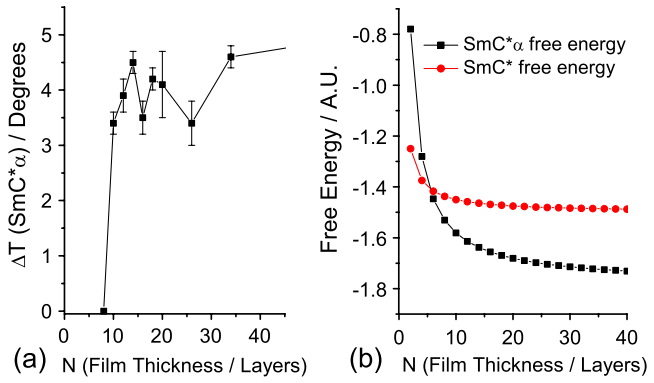

FIG. 4 (color online). (a) ΔT(SmC^*_α) as a function of N (b) free energy per layer of the SmC^*_α structure (black squares) and SmC^* structure (red dots) as a function of film thickness calculated from Eq. (1).

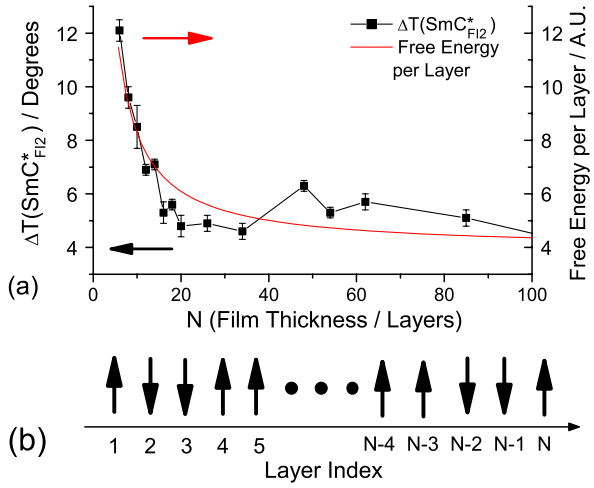

FIG. 5 (color online). (a) ΔT(SmC^*_{FI2}) as a function of N (black square) and free energy per layer calculated with Eq. (2) (red line). (b) Cartoon of a film with even number of layers in the SmC^*_{FI2} phase.

stability of the phase. Figure 5(b) shows a cartoon of the SmC^*_{FI2} structure of a film with even number of layers. Since the distortion angle δ_2 of MHPBC is small ($10° \pm 2°$), a planar structure (Ising-like) is a good approximation. The two outermost surface layers are assumed to be anticlinic with the neighboring layers as obtained from the fitting shown in Fig. 2(b).

Taking into account the fact that surface bonds are usually stronger than interior bonds, we write the coupling strength between the surface and the adjacent layer to be $-\gamma J_1$ [in the SmC^*_{FI2} phase $J_1 < 0$, so here a negative sign is needed to produce the anticlinic surface arrangement shown in Fig. 5(b)]and γJ_2 stands for the coupling strength between the surface and the NNN, with γ (a constant) representing the level of surface enhancement. Thus, for the structure shown in Fig. 5(b), including a NN and NNN interaction, we have

$$\begin{aligned} |F(\mathrm{Sm}C^*_{FI2})|/N &= \Big|\Big(\sum_{i=2}^{N-2} J_1 \boldsymbol{\xi_i}\cdot\boldsymbol{\xi_{i+1}} + \sum_{i=2}^{N-3} J_2 \boldsymbol{\xi_i}\cdot\boldsymbol{\xi_{i+2}} \\ &\quad - 2\gamma J_1 \boldsymbol{\xi_1}\cdot\boldsymbol{\xi_2} + 2\gamma J_2 \boldsymbol{\xi_1}\cdot\boldsymbol{\xi_3}\Big)\Big|\Big/N \\ &= J_2 + [2\gamma(J_2 - J_1) - (4J_2 + J_1)]/N \\ &= a + b/N \end{aligned} \tag{2}$$

with J_1 (J_2) term standing for the interior NN (NNN) interaction, and $\boldsymbol{\xi_i}$ representing the tilt direction of layer i, $a = J_2$, and $b = [2\gamma(J_2 - J_1) - (4J_2 + J_1)]$. The red line in Fig. 5(a) was obtained with $a = 3.9 \pm 0.3$ and $b = 43 \pm 3$. Using $J_1 = -2.5J_2$ as determined from the SmC^*_α structure, we obtain $\gamma = 1.8$. If, however, we follow the constrains in the ANNNI model for the SmC^*_{FI2} structure, $-J_1 < 2J_2$ [4], then we have $\gamma > 2.2$, which is reasonable for the case of AFLC [23]. These results show that the dramatic increase of $\Delta T(\mathrm{Sm}C^*_{FI2})$ in thin films is the result of enhanced coupling strength at the surface. Structure of the SmC^*_{FI2} phase allows both the NN bonds and the NNN bonds of the surfaces to contribute to the enhancement of stability of this phase, causing the effect to be more pronounced. For the case of SmC^*_A which also has an Ising-like structure, these two interactions will work against each other, causing the effect to be less obvious. With $J_1 = 2.5J_2$ and $\gamma = 2$, we get $\Delta T(\mathrm{Sm}C^*_A)$ increases for about 26% in decreasing N from 100 to 6 layers, much less compared to about 200% for SmC^*_{FI2}. Since in SmC^*_A, $J_1 > 0$, the γJ_1 term will not need a negative sign. Note the current model [Eq. (2)] does not apply to the case of SmC^*_α. More advanced models are required to explain all the experimental findings.

In summary, we studied the thickness dependent phase diagram of free standing films of AFLC compound MHPBC. The SmC^*_α phase disappears below a film thickness of 10 layers, which is of the order of the bulk helix. In thinner films the SmC^* structure is observed below SmA. This result is attributed to the reduced coordination number of the surface layers and is consistent with studies on helically ordered magnetic system. The temperature window of the SmC^*_{FI2} phase increases dramatically upon reducing the film thickness. Surface enhanced couplings are found to be the key reason. The ratio γ of the enhanced surface couplings to the bulk ones is found to be around 2.

Because of the similar structures in both systems, studies on magnetic thin films are proven to be valuable resources for our understanding of SmC^* variant phases. However, the relatively easy preparation of AFLC films with desired thicknesses and the rich phase behaviors make them more accessible for experimental studies. Also, the completely different surface effects in the two systems (surface induced order for AFLC films and surface induced disorder for magnetic thin films) make the comparison between the two systems even more interesting, and will enhance our understanding of the roles of surface in systems having layered structures.

This research was supported in part by the National Science Foundation, Solid State Chemistry Program, under Grant No. DMR-0605760.

[1] A. D. L. Chandani *et al.*, Jpn. J. Appl. Phys. **28**, L1265 (1989).
[2] P. Mach *et al.*, Phys. Rev. Lett. **81**, 1015 (1998).
[3] P. M. Johnson *et al.*, Phys. Rev. Lett. **84**, 4870 (2000); D. Konovalov *et al.*, Phys. Rev. E **64**, 010704(R) (2001); M. Škarabot *et al.*, Phys. Rev. E **58**, 575 (1998).
[4] M. E. Fisher and W. Selke, Phys. Rev. Lett. **44**, 1502 (1980).
[5] A. Roy and N. V. Madhusudana, Eur. Phys. J. E **1**, 319 (2000).
[6] D. A. Olson *et al.*, Phys. Rev. E **66**, 021702 (2002).
[7] M. Čepič *et al.*, J. Chem. Phys. **117**, 1817 (2002).
[8] P. V. Dolganov *et al.*, Phys. Rev. E **67**, 041716 (2003).
[9] M. B. Hamaneh and P. L. Taylor, Phys. Rev. Lett. **93**, 167801 (2004); Phys. Rev. E **72**, 021706 (2005).
[10] C. Y. Chao *et al.*, Phys. Rev. Lett. **86**, 4048 (2001).
[11] E. I. Demikhov, JETP Lett. **61**, 977 (1995).
[12] L. D. Pan *et al.*, Phys. Rev. E **79**, 031704 (2009).
[13] P. M. Johnson *et al.*, Phys. Rev. Lett. **83**, 4073 (1999).
[14] B. K. McCoy *et al.*, Phys. Rev. E **73**, 041704 (2006).
[15] D. A. Olson *et al.*, Liq. Cryst. **29**, 1521 (2002).
[16] D. Schlauf *et al.*, Phys. Rev. E **60**, 6816 (1999).
[17] D. W. Berreman, J. Opt. Soc. Am. **62**, 502 (1972).
[18] A. Fera *et al.*, Phys. Rev. E **64**, 021702 (2001).
[19] P. V. Dolganov *et al.*, Phys. Rev. E **65**, 031702 (2002).
[20] E. Weschke *et al.*, Phys. Rev. Lett. **93**, 157204 (2004).
[21] F. Cinti *et al.*, Phys. Rev. B **78**, 020402(R) (2008).
[22] D. A. Olson *et al.*, Phys. Rev. E **63**, 061711 (2001).
[23] K. Binder and P. C. Hohenberg, Phys. Rev. B **9**, 2194 (1974).